



AUTHOR(S):

TITLE:

YEAR:

Publisher citation:

OpenAIR citation:

Publisher copyright statement:

This is the _____ version of proceedings originally published by _____
and presented at _____
(ISBN _____; eISBN _____; ISSN _____).

OpenAIR takedown statement:

Section 6 of the "Repository policy for OpenAIR @ RGU" (available from <http://www.rgu.ac.uk/staff-and-current-students/library/library-policies/repository-policies>) provides guidance on the criteria under which RGU will consider withdrawing material from OpenAIR. If you believe that this item is subject to any of these criteria, or for any other reason should not be held on OpenAIR, then please contact openair-help@rgu.ac.uk with the details of the item and the nature of your complaint.

This publication is distributed under a CC _____ license.

Numerical investigation of two-phase flow induced local fluctuations and interactions of flow properties through elbow

Nkemjika Chinenye-Kanu, Mamdud Hossain, Mohamad Ghazi Droubi, and Sheikh Zahidal Islam

School of Engineering, Robert Gordon University, Aberdeen, AB10 7GJ, United Kingdom.

n.m.chinenye-kanu@rgu.ac.uk, m.hossain@rgu.ac.uk, m.g.droubi@rgu.ac.uk, s.z.islam1@rgu.ac.uk

Abstract. The local interactions and fluctuations of multiphase flow properties present in upward slug/churn flow patterns through a 90° pipe bend has been investigated. Numerical modelling technique using the Volume of Fluid method (VOF) and Reynolds Averaged Navier-Stokes equation (RANS) was used in this study. Validation of the modelling approach was carried out using the void fraction signals from the simulation and its PDF result. These signals compared well with reported experimental results for slug and churn flow patterns. Result analysis which focused on velocity and pressure fluctuations at three different cross-sectional planes of the elbow showed a reduction in the fluctuation energy (PSD) of the velocity signal at the downstream locations compared to the upstream. Similar behaviour was seen in the pressure signal. The observation was attributed to the change in multiphase flow patterns from slug to stratified/stratified wavy flow pattern after the bend. The results from this study intend to inform enhanced description of the local fluctuations of slug geometry, density and frequency for the accurate prediction of flow induced fluctuating forces due to slug-churn turbulent flows at pipe bends.

Keywords: CFD, void fraction, pressure and velocity variations, flow induced local fluctuations, flow properties interactions

1 Introduction

Internal multiphase flow induced vibration (FIV) has increasingly become a recent flow assurance and structural integrity concern in the oil and gas production and process industry. Different sections of the oil and gas facilities including the subsea risers, manifolds, jumpers, undulating pipeline spans on seabeds and top-side process and transporting systems contain complex geometries such as bends and tees which are sources of FIV [1]. The fluctuating hydrodynamic properties due to dynamic internal multiphase flows can modify natural frequencies and modes of vibration of structures [2]. Vibrations could potentially lead to

resonance, fatigue cracks, fractures, wear or total failure of structures. Assumptions in describing the instantaneous internal multiphase flow parameters that would introduce error in predictions of the internal flow induced forces frequency and magnitude could easily misinform flowline designs against resonance effect or fatigue. A multiphase FIV study identified the momentum flux and normal pressure in the direction of flow as the main sources of the flow induced force due to upward two-phase flow through a pipe bend [3]. Further investigation concluded that an impact force component has a significant contribution to the total fluctuating force particularly in cases of slug and moderate churn flow patterns [4]. Mathematical modelling of the fluctuating impact force term showed the dependence of slug/churn flow induced forces on the flow pattern characteristics which include bubble distribution and sizes, interfacial area concentration and roughness parameter. This indicates that accurate quantitative and qualitative description of the characteristics and behaviour of slug and churn flow at pipe bends is very crucial to formulating accurate FIV predictive models.

Experimental studies [5–7] have been conducted in attempt to explore the transient interactions between phases in two-phase flows. A more detailed study investigated the evolution of slug and churn gas pockets using a multivariate pseudo Wigner distribution together with multivariate multiscale entropy to analyse the measured data [5]. The study could be useful for validation purposes but it is limited by the flow geometry (0.02m diameter) and conditions (low velocities) it could cover in the experiment. In addition, a number of studies have applied the computational fluid dynamics methods (CFD) to observe the characteristic behaviours of slug and churn flow patterns. Gayet et al. [8] simulated a single Taylor bubble flow in a vertical U-shaped spool (ID. = 0.1524m, bend radius = 0.762 m) to observe pressure variations. On the other hand, Emmerson et al. [9] studied full slug flow in horizontal pipes of diameters 0.1016 m and 0.070 m having bend configurations of 180-degree and 90-degree, respectively. The study by Emmerson et al. [9] reported an interaction in the x-direction forces at upstream and downstream positions of the 180° bend but didn't offer more insight into the flow properties fluctuations that contributed to the force interaction between the two positions. Also, studies have investigated churn flows through a pipe elbow (ID. = 0.0762 m) using CFD modelling approach [10, 11]. The former [10] equally simulated a horizontal version of the pipe geometry in which it observed a form of slug/pseudo slug flow. Furthermore, studies show that the volume of fluid (VOF) model in CFD performs well for slug flow modelling [8, 9, 12, 13] and in churn flow modelling [14]. Ratkovich et al. [15] who also used VOF model to simulate slug flow reported that CFD results compared fairly well with both experimental data and empirical correlations. RANS models has been satisfactorily applied to model turbulence in slug and churn flow [10, 12].

In addition to the pressure variation study [8] due to a single Taylor bubble, experiment by Nakamura et al. [16] observed the presence of local pressure fluctuation and flow separation at pipe elbow due to turbulent single phase flow. The study [16] confirmed that the observed behaviour affected the random flow induced vibration force at the bend. Pressure variation due to a single

bubble could considerably differ from the variations due to continuous slug and churn flows while pressure fluctuation due to single phase flow could also differ from slug and churn flow due to the inherent dynamic behaviours in such flows. Also, distortion of the slugs and churn bubbles in upward flow through bends increases the difficulty to mechanistically or analytically describe the accurate interfacial surface area [4, 17] between phases at the elbow and in the rest of the flow domain. Therefore, assumptions in local fluctuations of pressure, density (void fraction), geometry and slug frequency based only on the presented studies could easily yield unsatisfactory prediction of slug and churn flow induced forces at pipe bends.

More in-depth CFD studies will increase better understanding of the important dynamic behaviours and interactions due to the present flow patterns at a bend. This study applied numerical modelling technique to focus on detailed qualitative and quantitative analysis of the time domain signals of the fluctuating flow properties at entrance and exit of the pipe bend. The analysed transient pressure, velocity and void fraction signals obtained from the converged solutions of validated CFD simulations of slug and churn flows were presented and discussed.

2 Numerical modelling

2.1 Two-phase flow model

The flow conditions in the present study are governed by the equations of adiabatic flow of compressible fluid given as the continuity and momentum conservation equations. The continuity and momentum equations are given in [18] as Equation 1 and Equation 2 respectively as:

$$\frac{\partial \rho}{\partial t} + \frac{\partial \rho u_i}{\partial x_i} = 0 \quad (1)$$

$$\frac{\partial \rho u_j}{\partial t} + \frac{\partial \rho u_i u_j}{\partial x_i} = -\frac{\partial P}{\partial x_j} + \frac{\partial}{\partial x_i} \mu \left(\frac{\partial u_i}{\partial x_j} + \frac{\partial u_j}{\partial x_i} \right) + \rho g_j + F_j \quad (2)$$

Solving the continuity equation for the volume fraction of each phase during the simulations, tracks the interface between the phases. Assuming no mass transfer, the equation is given as [18]:

$$\frac{\partial(\alpha_q)}{\partial t} + \frac{u_i \partial(\alpha_q)}{\partial x_i} = 0 \quad (3)$$

where the subscript 'q' stands for each phase and all the phases volume fractions equals to unity in each computational cell. All variables and properties of the contents of each cell represent a volume averaged value and depends on the volume fractions of the phases. For instance the dynamic viscosity of the contents of each cell is given as:

$$\mu = \alpha_a \mu_a + \alpha_w \mu_w \quad (4)$$

The same operation (Equation 4) is applicable to density. The method known as Geo-reconstruct[19] has been applied in the numerical simulation tool to accurately predict the exact position, orientation and slope of interfaces in the cases of cells containing both liquid and gas phases.

2.2 Turbulence model

This study applied the RANS approach to account for turbulence in the flow. The equation is given by [20] as:

$$\rho\left(\frac{\partial \bar{u}_i}{\partial t} + \bar{u}_k \frac{\partial \bar{u}_i}{\partial x_k}\right) = -\frac{\partial \bar{p}}{\partial x_i} + \frac{\partial}{\partial x_j}\left(\mu \frac{\partial \bar{u}_i}{\partial x_j}\right) + \frac{\partial(-\rho \overline{u_i' u_j'})}{\partial x_j} \quad (5)$$

The two-equation k - ϵ models calculate for the extra unknowns in the RANS equation in order to close the system of equations. The k - ϵ equations for turbulent kinetic energy k and its dissipation ϵ are given by [21] respectively as:

$$\rho u_j \frac{\partial k_m}{\partial x_j} = \frac{\partial}{\partial x_j}\left(\frac{\mu_{tm}}{\sigma_k} \frac{\partial k_m}{\partial x_j}\right) + \mu_{tm} \frac{\partial u_j}{\partial x_i} \left(\frac{\partial u_i}{\partial x_j} + \frac{\partial u_j}{\partial x_i}\right) - \rho \epsilon_m \quad (6)$$

$$\rho u_j \frac{\partial \epsilon_m}{\partial x_j} = \frac{\partial}{\partial x_j}\left(\frac{\mu_{tm}}{\sigma_\epsilon} \frac{\partial \epsilon_m}{\partial x_j}\right) + C_1 \mu_{tm} \frac{\epsilon_m}{k_m} \frac{\partial u_j}{\partial x_i} \left(\frac{\partial u_i}{\partial x_j} + \frac{\partial u_j}{\partial x_i}\right) - C_2 \frac{\epsilon_m^2}{k_m} \rho \quad (7)$$

where,

$$\mu_t = \rho C_m u \frac{k^2}{\epsilon} \quad (8)$$

The constants C_μ , σ_k , σ_ϵ , $C_{1\epsilon}$ and $C_{2\epsilon}$ are given as 0.9, 1.0, 1.3, 1.44 and 1.92 respectively. Finally, the first grid cell height y is calculated by:

$$y = \frac{y^+ \mu}{U_\tau \rho} \quad (9)$$

where $30 < y^+ < 300$.

3 Solution approach

The computational domain and flow conditions is similar to the experimental set-up of [3] which is an upward flow in vertical 90° elbow of diameter 0.0525m and radius of curvature of 0.0762m. The lengths of the upstream and downstream branches of the elbow were 4m each. The meshes which were used to conduct the mesh independent study are also shown in Figure 2. 7 slug/churn flow cases shown in Table 1 (according to the Mishima and Ishii's transition flow regime map) were simulated.

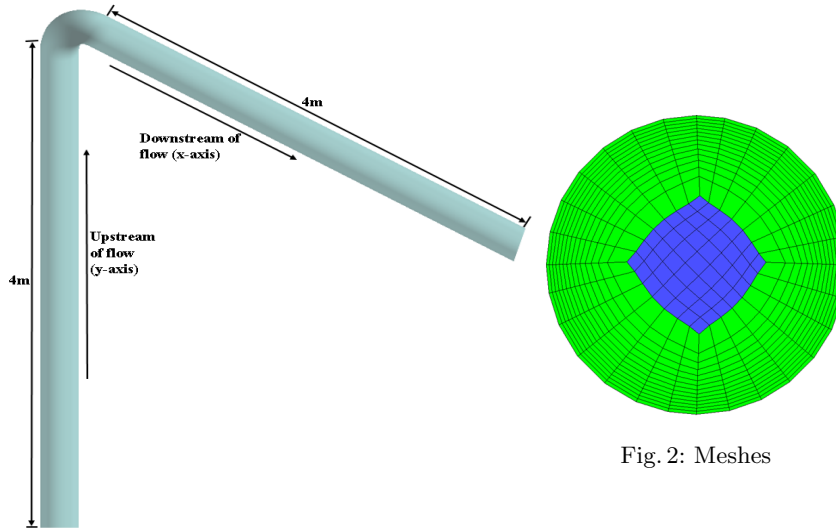


Fig. 1: Pipe Geometry

Fig. 2: Meshes

The transient simulations are carried out in pressure-based solver. A negative vertical upward gravity ($-9.81ms^{-2}$) is specified. Under the VOF model, the explicit scheme is used. The surface tension between the two fluids was set as a constant of $0.0728N/m$. Also, implicit body force formulation is used. The turbulence is modelled with RANS standard $k - \epsilon$ and the standard wall function was applied. Water was assigned as the primary phase (phase 1) while air was assigned the secondary phase (phase 2). The SIMPLE scheme was used for pressure-Velocity coupling. The spatial discretization for pressure, momentum and volume fraction were selected to be PRESTO, second order upwind and Geo-Reconstruct respectively. In the cases of turbulent kinetic energy and dissipation rate first order upwind were selected. Also first order implicit transient formulation was adopted. All residuals were set to 0.001. The under-relaxation factors for; pressure, density, body forces, momentum, turbulent Kinetic energy, turbulent dissipation rate and turbulent viscosity are given as 0.3, 1, 0.5, 0.3, 0.6, 0.6, 0.5 respectively. Finally, a fixed time step of 0.0001s or 0.00001s were used for a maximum iteration of 50.

4 Results and Discussion

4.1 Boundary and initial condition

The pipe inlet which was set as velocity inlet was split in two for air (center-blue colour) and water (outer area- green colour) as shown in Figure 2. The pipe outlet was set as pressure-outlet. The fluids are initially introduced into the flow

domain at the inlets by setting the phase velocities. The gas and liquid phase velocities are calculated respectively as:

$$V_g = \frac{V_{sg} \times A_T}{A_g} \quad (10)$$

$$V_l = \frac{V_{sl} \times A_T}{A_l} \quad (11)$$

Table 1 presents the calculated inlet phase velocities corresponding to the superficial velocities for each case study.

Table 1: Simulation Cases

Cases	V_{sg} [m/s]	V_{sl} [m/s]	V_g [m/s]	V_l [m/s]
1	0.773	0.642	4.89	0.763
2	0.978	0.642	6.189	0.763
3	1.7	0.642	10.76	0.763
4	2.765	0.642	17.5	0.763
5	9.04	0.642	57	0.763
6	0.978	0.61	6.189	0.725
7	9.04	0.61	57	0.725

4.2 Phase distribution and velocity variation

A slug (case 6) and churn (case 7) flow case studies with similar superficial velocities reported by Liu et al.[3] were initially simulated. The results were used to carry out mesh sensitivity studies as well as validation studies. The mesh shown in Figure 2 having a mesh cells of 366912 produced the optimum result for void fraction signal considering both accuracy and computer resources. Figure 3 presents the void fraction signals for cases 6 and 7 in actual flow time. The trends in both plots were observed to conform with the reported study by Liu et al.[3] for the same gas and liquid superficial velocities. The slug flow signal is seen to represent a typical intermittent flow of gas and liquid slugs. The churn flow signal also shows a more chaotic flow with longer and irregular shaped gas columns while the liquid phase is observed to rarely bridge the pipe cross-section. A PDF analysis of both signals (Figure 4) conformed to the observation in the raw signals of both the slug and churn flows. The PDF analysis for slug flow showed two important peaks at $\alpha=0.1$ and 0.7 [-] representing the liquid and gas slugs respectively. On the other hand, the churn flow is observed to have one distinct peak at $\alpha=0.89$ [-] representing the long wavy gas columns with occasional liquid (filled with bubbles) bridges that were more consistent in the flow. The results of the PDF analysis also agree with the observations reported in literature by Lowe and Rezkallah [22] and Costigan and Whalley [23] for slug and churn flow patterns.

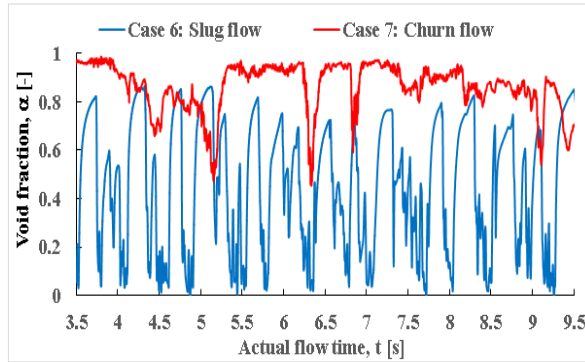


Fig. 3: Void fraction signal for case 6 and 7

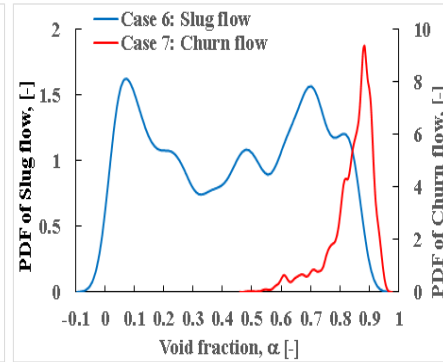


Fig. 4: PDF of void fraction

The control volume shown in Figure 5 was created at the elbow. The following presented results and discussions are based on data extracted from the control volume. Figures 6, 7 and 8 show typical qualitative visualizations of void fraction contour, isosurface (taken at $\alpha=0.85$) and velocity stream lines of the churn flow case 7. As flow time increased from 10.79s to 10.806s, light wisps of liquid film detaching from long upward churn flow waves along the vertical pipe were observed to temporarily accumulate at the elbow (Figures 6) but could hardly bridge the pipe diameter. The visualized detachment of liquid film agree with literature in which large waves structures were reported to eventually breakup to form droplets [24] or according to Da Riva and Del Col [14], liquid peel off from the wave to form finger-like shapes in the flow. In the present study, the momentary accumulation of the film downstream at the elbow is attributed to the reduced flow velocity due to instantaneous impact of the films on the upper section (extrados) of the inner wall of the bend towards the horizontal pipe section. The drop in stream velocity due to the liquid film behaviour is also visible from the streamlines of the flow (Figure 8). The green streamlines indicate a lower velocity compared to the red coloured mid stream velocity.

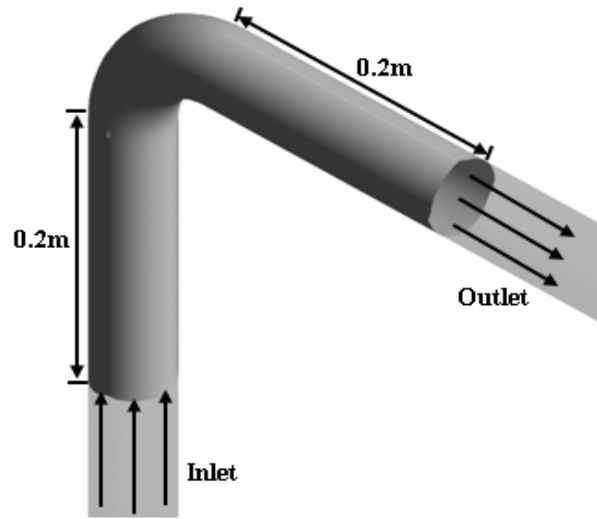


Fig. 5: Control volume

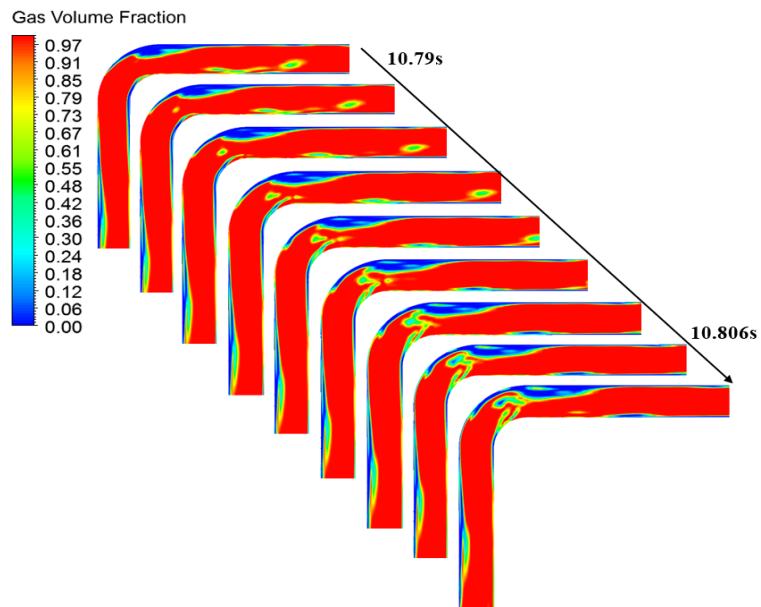


Fig. 6: Typical void fraction contour of case 7 at 10.79s to 10.806s of flow time

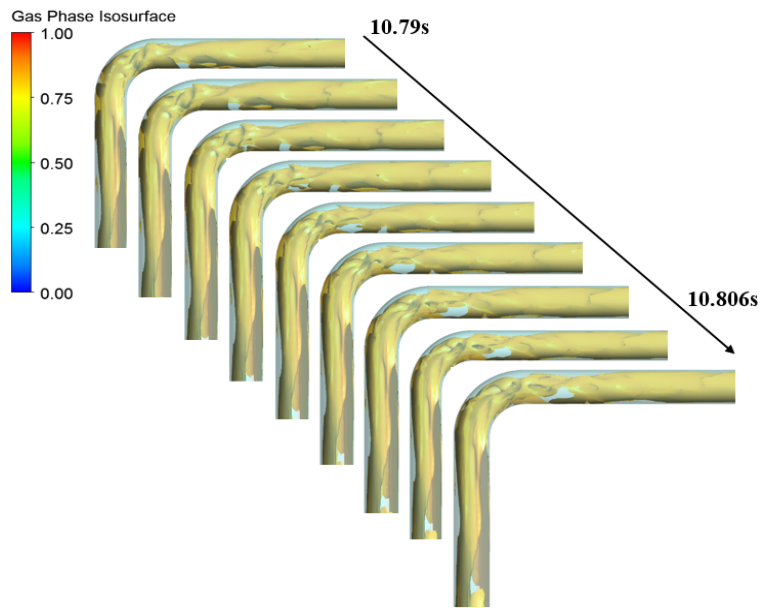


Fig. 7: Isosurface (0.85) of case 7 for 10.79s to 10.806s of flow time

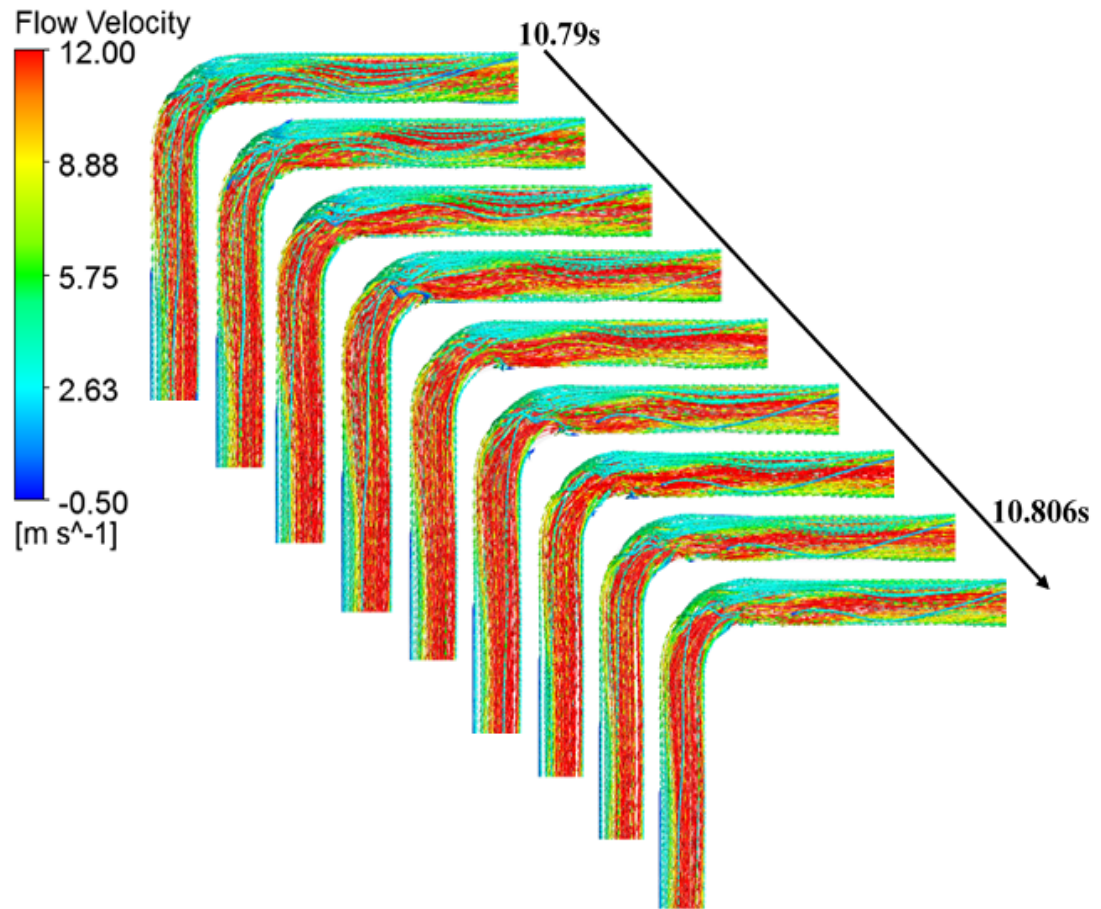


Fig. 8: Streamlines of case 7 for 10.79s to 10.806s of flow time

In case 6, the stream lines (Figure 10) show some reversed flow of the liquid film surrounding the Taylor bubble (Figure 9) along the vertical (upstream) pipe section just before the bend. The reversed flow behaviour supports the falling film observation in the experiment by Abdulkadir [12]. In this study, the behaviour could have been enhanced within the present control volume by the slower moving flow due to instantaneous impact of the preceding liquid slug at the bend. Flow separation and what appears to be a vortical streamline structure was also seen at the inner (intrados) section of the horizontal pipe immediately downstream of the bend at similar location where Nakamura et al. [16] observed separation in the case of single phase flow. As the Taylor bubble fills the elbow more chaotic streamlines are observed (Figure 10). The observation is due to the surrounding liquid film dropping under the effect of gravity while simultaneously in a forward flowing motion along the horizontal pipe section. Further

downstream, the dropping liquid tends to form a bed while the faster moving gas phase rises to the top as obtainable in stratified-wavy flows with the waves nearly bridging the pipe occasionally. The experimental report by Abdulkadir et al. [25] supports the observation in this study that the phase distribution of a vertical upward slug flow changes to stratified wavy flow after a 90° bend, although the superficial velocities in the report were less than the velocities in the present study.

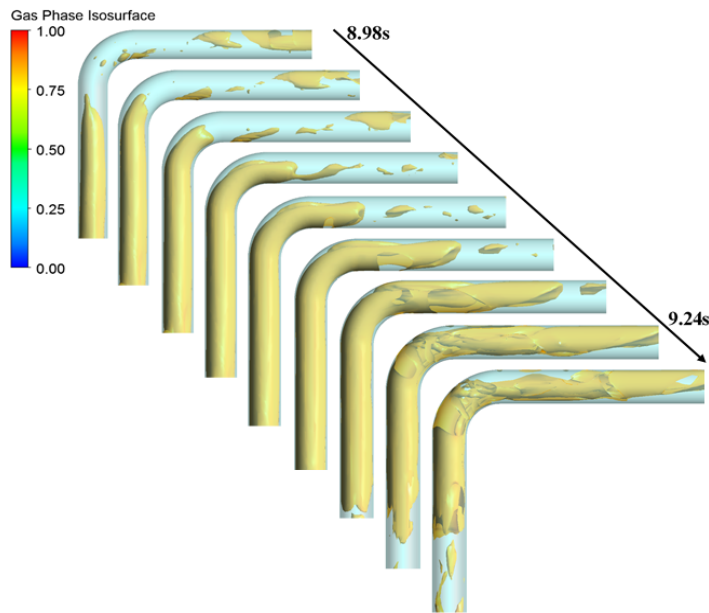


Fig. 9: Isosurface (0.85) of case 6 for 8.98s to 9.24s of flow time

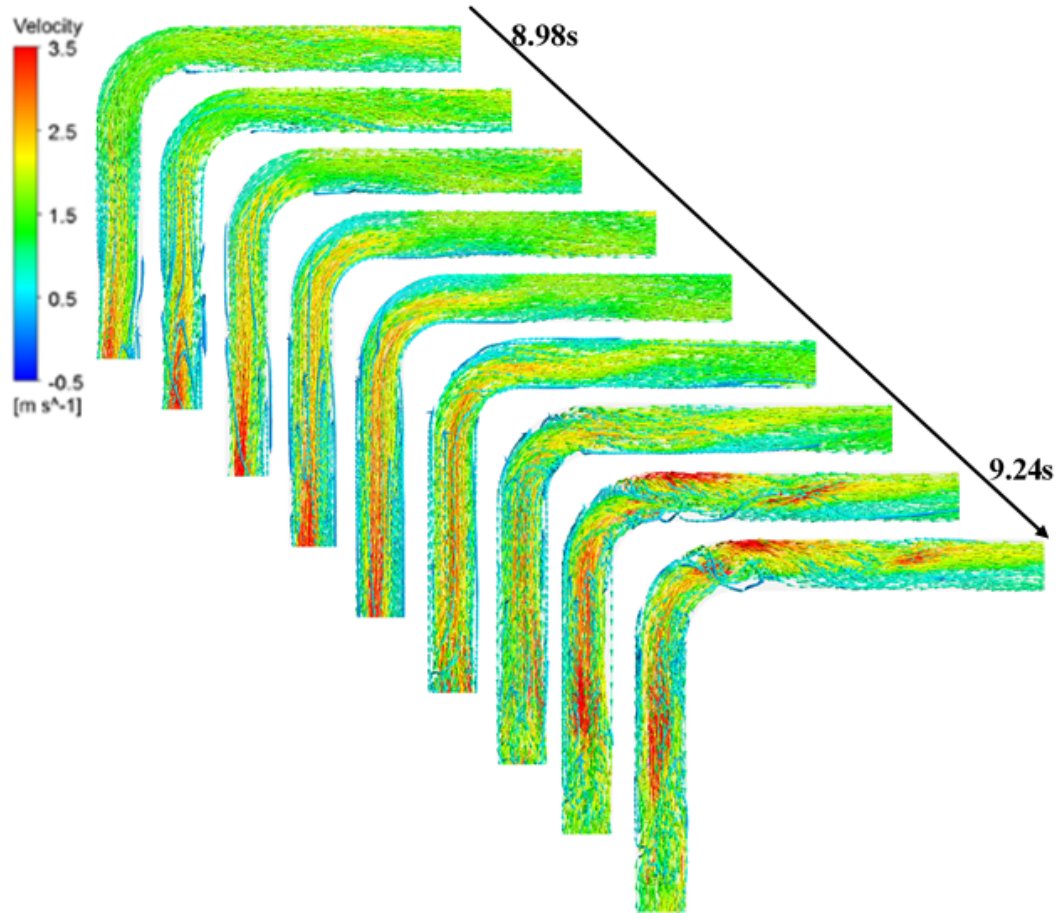


Fig. 10: Streamlines of case 6 for 8.98s to 9.24s of flow time

The time domain velocity data were obtained from cross sectional planes created at the inlet of the control volume in Figure 5, at an angle of 45° across the 90° elbow and at the outlet of the control volume. More important fluctuations about mean value were observed in the x and y components of velocity at the 45° plane than were observed for the inlet and outlet planes. Although, the signal obtained at the outlet plane presented less fluctuation about the mean value compared to the signal at the inlet. Also, the fluctuations generally dropped as gas superficial velocities increased from slug to churn flow conditions. In Figure 12 and 13 the PSD analysis of the signals show that the fluctuating velocity signal also varied in both the fluctuation energy and frequency from inlet plane to exit plane of the control volume. The fluctuation energy is found to be higher in the upstream location than the horizontal downstream location. The figures also show that the peak and other equally important PSD of velocity fluctuation

are within the 0 - 10 Hz frequency band for the inlet plane while the outlet plane PSD are more distributed within 0 - 50Hz.

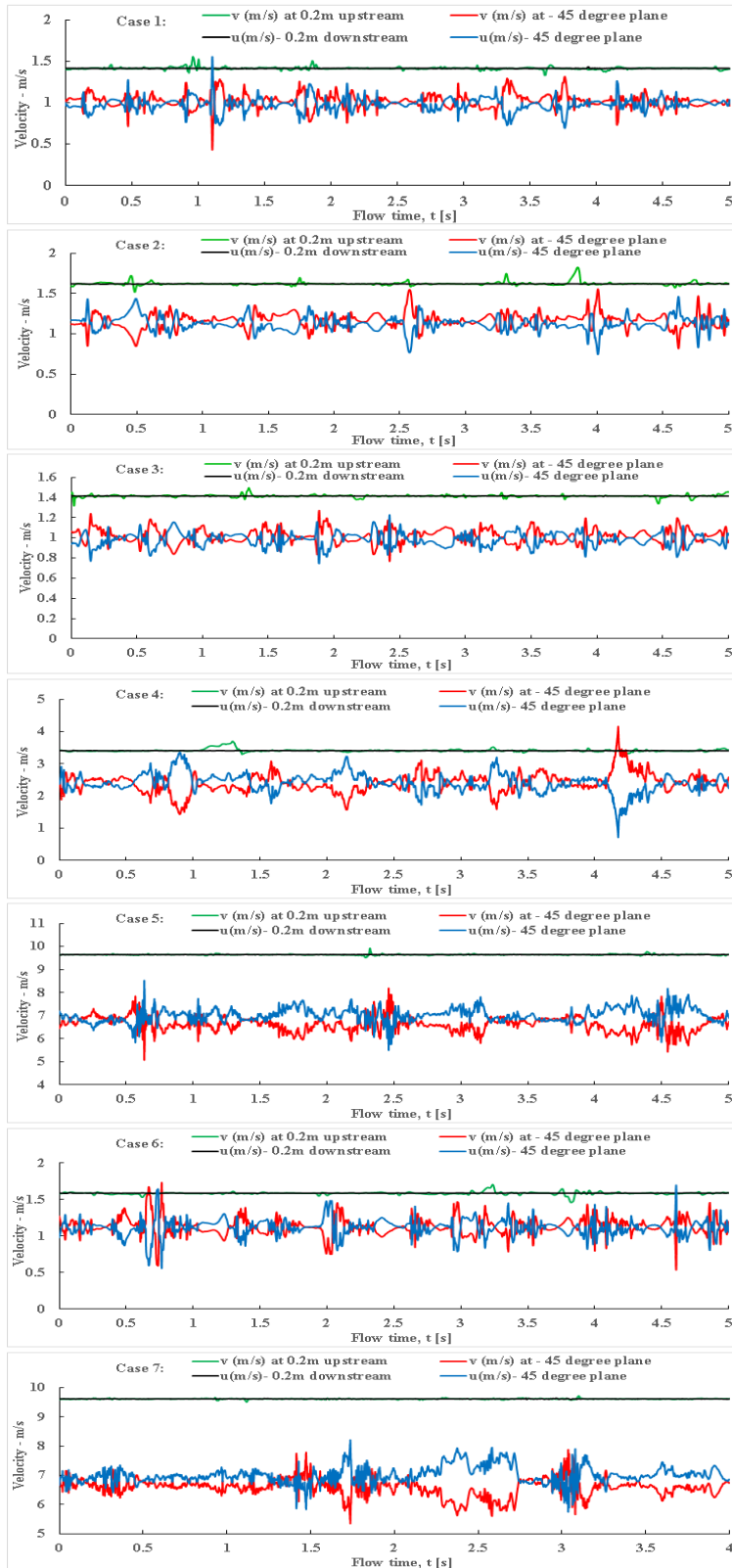


Fig. 11: Velocity fluctuations and local variations for all case studies

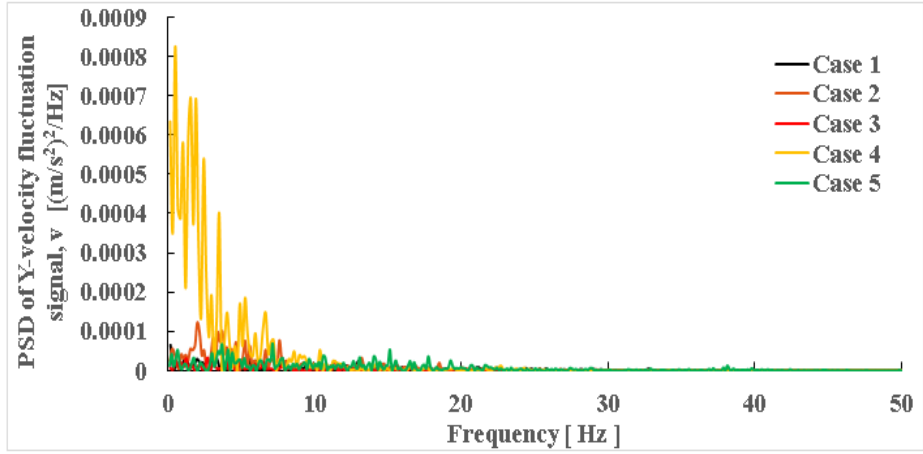


Fig. 12: PSD analysis of the y-direction (v) mixture velocity at upstream of bend

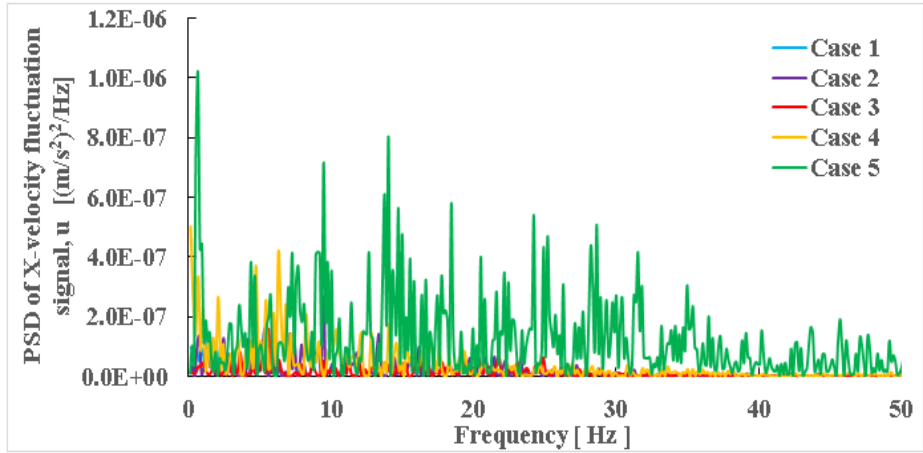


Fig. 13: PSD analysis of the x-direction (u) mixture velocity at downstream of bend

4.3 Pressure

The pressure contour on the pipe wall for case 7 shown in Figure 14 show that an interaction exist between the pressure distribution at the bend location and the momentary accumulation of liquid film at the same location presented in Figures 6. The pressure intensity increased as the liquid film thickness increased.

Figure 15 shows that the pressure fluctuation signal due to the two-phase flow also varied from the control volume inlet plane to the outlet plane. In the slug

flow cases 1, 2, 3 and 6 the trend of the signals obtained at the inlet plane exhibited similar behaviour with typical slug flow void fraction signal showing visible crests and trough due to alternating passage of gas and liquid slugs through the cross sectional plane. Such behaviour was not present with higher gas superficial velocities in case 4 and churn flow cases 5 and 6. The signal behaviour that was observed at the inlet plane for the slug flow cases was no longer present at the outlet plane. The variation is associated with the change in flow pattern from slug flow with Taylor bubbles to stratified wavy flow in the horizontal pipe downstream of the bend. The churn flow cases generally showed less fluctuations/intermittency due to the more chaotic nature leading to better mixing of the two phases than is obtainable in the highly intermittent slug flows.

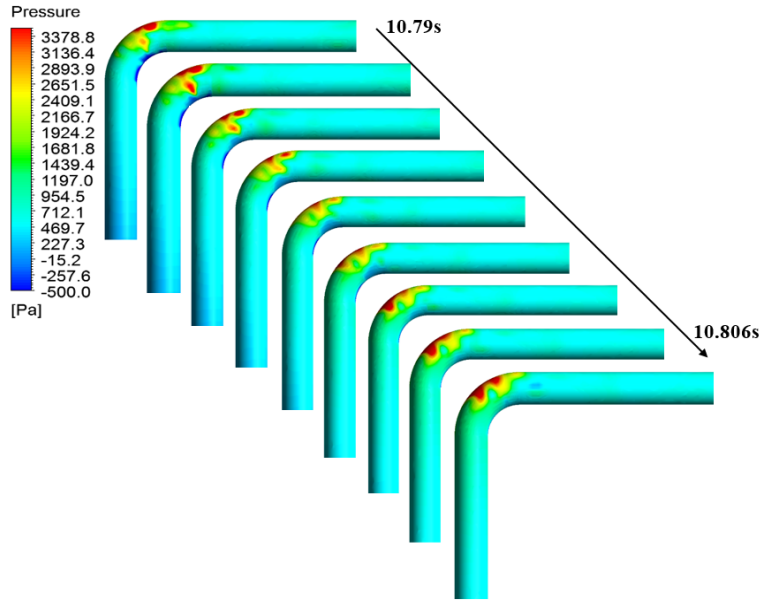


Fig. 14: Pressure contour for 10.79s to 10.806s of flow time

Due to local fluctuations in void fraction, density and pressure, negative pressure drops were observed between the inlet and outlet of the control volume. Figure 15 shows a close interaction between the void fraction signals and the pressure drop for all the two-phase case studies. At time 2s in case 1, the void fraction at the inlet plane was observed to be lower than the void fraction at the outlet plane and the result of pressure drop calculation gave a positive value. The plot of case 7 shows similar observation at 3.1s. The interaction between the local fluctuations in void fraction signal and the pressure drop across the two planes were seen to remain consistent for all the two-phase flow case studies reported in the present study.

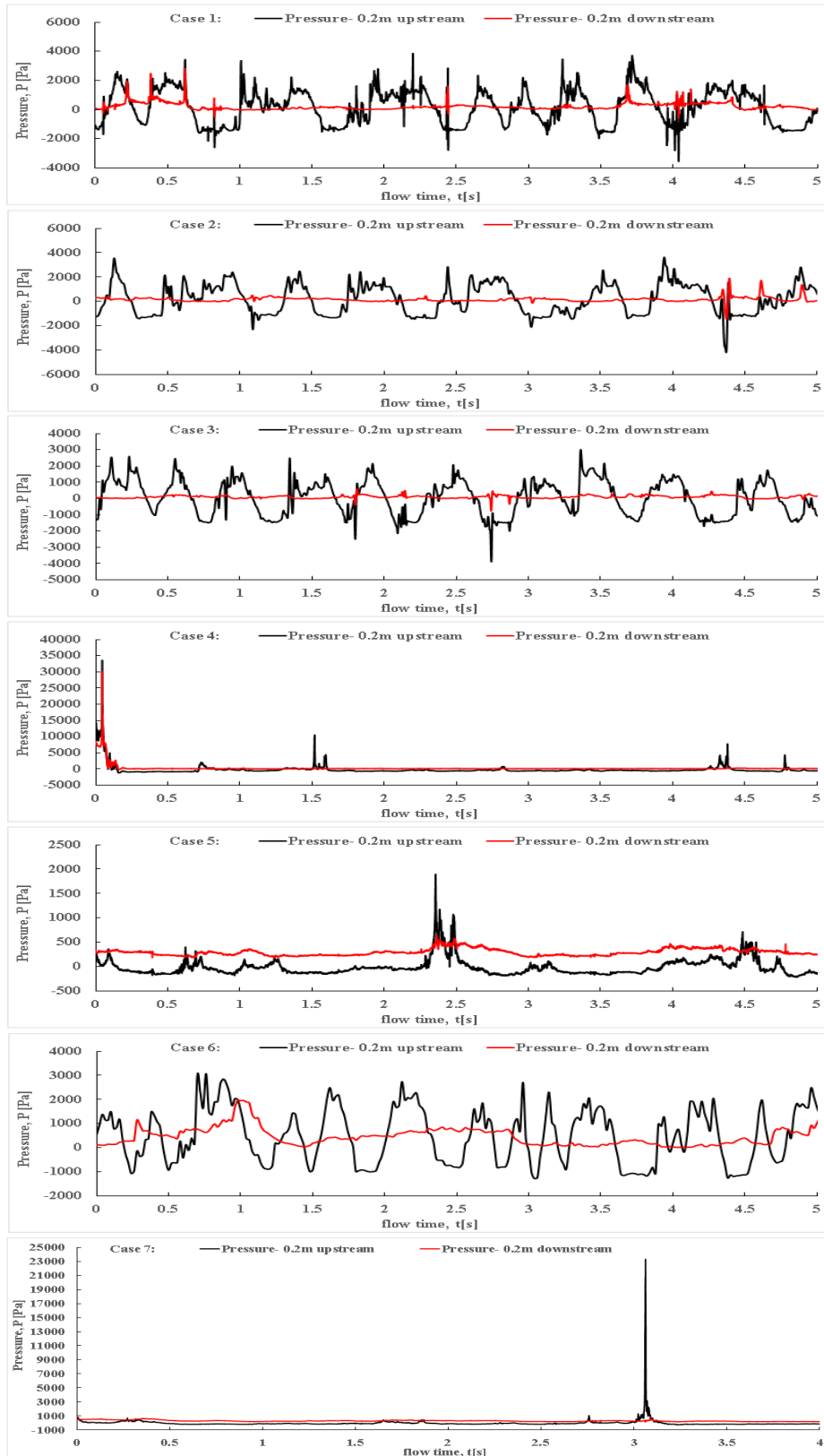


Fig. 15: Pressure fluctuations for all case studies

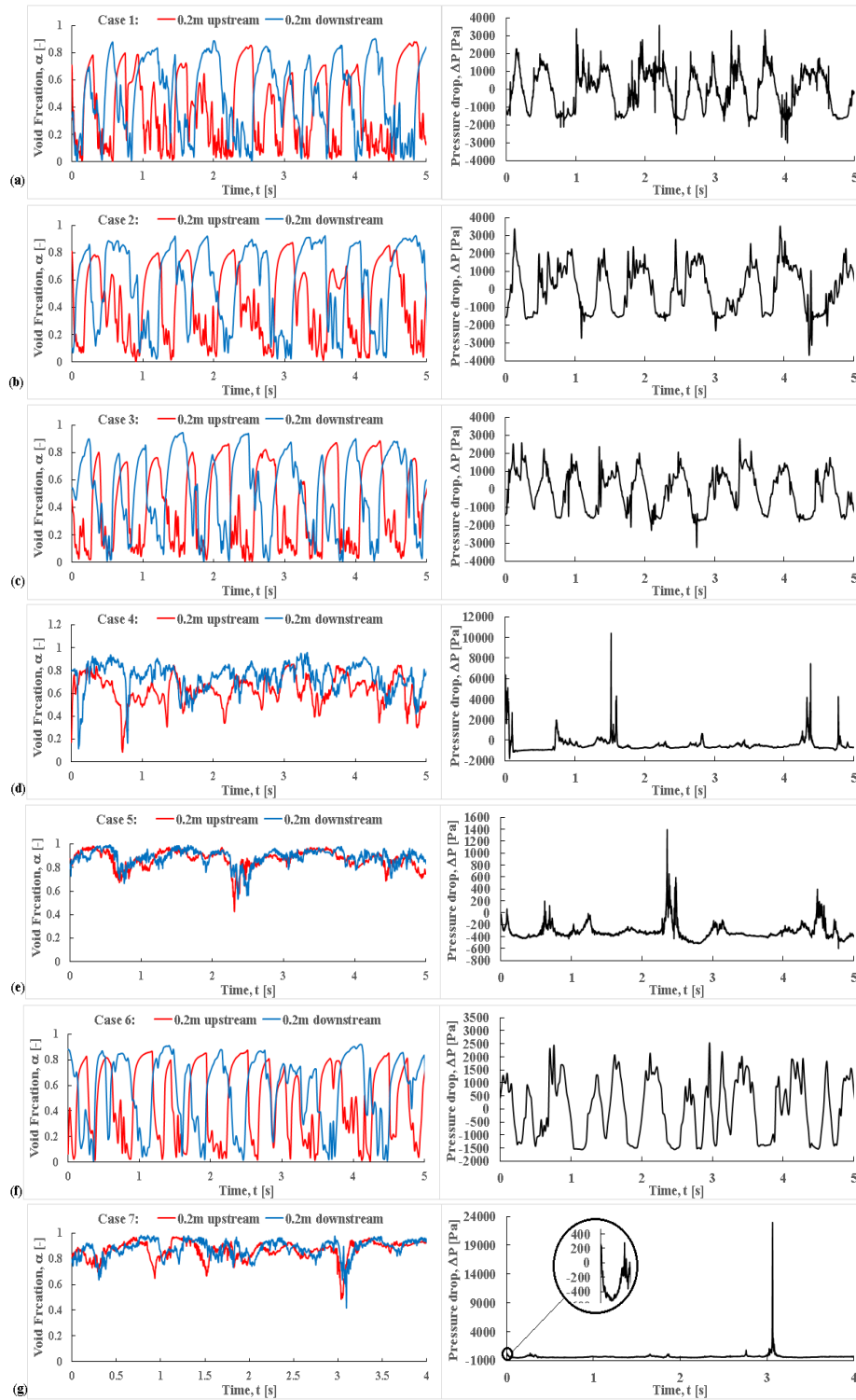


Fig. 16: Interaction between void fraction fluctuation and pressure drop across the bend control volume

5 Conclusion and Recommendation

This study has presented an indepth examination of the two-phase flow properties interactions and behaviours at a 90^0 bend due to local fluctuations in void fraction, flow velocity and pressure. The streamlines highlighted reversed flow of liquid film, flow separation and transition from slug flow to startified flow in the presented slug flow case. Likewise in the churn flow, the streamline and the contour plots of void fraction and pressure at the bend presented a qualitative visualization of the momentary accumulation of wisps of liquid film at the outer section (extrados) of the bend. Compared to the vertical and horizontal pipe sections, the time domain signal of the u and v velocity components at the bend showed a more unstable flow as the fluid changed direction. Futhermore, the results of the PSD analysis of the upstream and downstream velocity signals indicated that the fluctuation energy at the upstream location were higher than the down stream. Although, the most significant fluctuation energy were observed between 0 and 10Hz for the first 5 flow cases at the upstream pipe section. For the downstream, equally important fluctuation energy were present between 0 and 20Hz for slug flow with only the churn flow significant velocity fluctuation frequencies extending upto 50Hz. Pressure fluctuation signal generally showed a higher fluctuation upstream than downstream with more pronounced differenced in the moderate slug flow cases due to change in void fraction distribution from the upstream to the downstream positions. Interaction between the local fluctuations of void fraction and pressure drop was also established. Further study is expected to focus on investigating the existence of the presented two-phase flow interactions in large diameter pipes.

References

1. Gharaibah, E., Barri, M. and Tungen, R. Flow Induced Vibration for Design and Operation of Subsea Systems-State of the Art, Limitations and Potential Developments. Offshore Technology Conference Asia. Offshore Technology Conference (2016).
2. Meng, S., Kajiwara, H., Zhang, W. Internal flow effect on the cross-flow vortex-induced vibration of a cantilevered pipe discharging fluid, *Ocean Engineering*. 137, 120128, (2006).
3. Liu, Y., Miwa, S., Hibiki, T., Ishii, M., Morita, H., Kondoh, Y., Tanimoto, K. Experimental study of internal two-phase flow induced fluctuating force on a 90 elbow, *Chemical Engineering Science*. 76, 173187 (2012).
4. Miwa, S., Mori, M., Hibiki, T. Two-phase flow induced vibration in piping systems, *Progress in Nuclear Energy*. 78, 270284, (2015).
5. Gao, Z., Yang, Y., Zhai, L., Ding, M., Jin, N. Characterizing slug to churn flow transition by using multivariate pseudo Winger distribution and multivariate multiscale entropy. *Chemical Engineering Journal*. 291, 74-81 (2016).
6. Costa, C., Oliveira, P., Barbosa, J. Intermittent flow initiation in a horizontal tube: quantitative visualization and CFD analysis. *J. of the Brazilian Society of Mechanical Sciences and Engineering*, 40:188 (2018).

7. Pour, S. S., Mohanarangam, K., Vahaji, S., Cheung, S. C. P., Tu, J. Visualization of gas-liquid bubbly flows in a large diameter pipe with 90° bend
8. C. Gayet, M. Ndiaye, A. Lin, Behaviour of slug flow and pressure force induced in a spool: numerical simulation of a Taylor bubble flowing in a liquid flow through a spool, 16th International Conference on Multiphase Production Technology. BHR Group (2013).
9. P. Emmerson, M. Lewis, N. Barton, Improving boundary conditions for multiphase CFD predictions of slug flow induced forces, 17th International Conference on Multiphase Production Technology. BHR Group (2015).
10. M. Parsi, R. E. Vieira, M. Agrawal, V. Srinivasan, B. S. Mclaury, S. A. Shirazi, E. Schleicher, U. Hampel, Computational fluid dynamics (CFD) simulation of multiphase flow and validating using wire mesh sensor, 17th International Conference on Multiphase Production Technology. BHR Group (2015).
11. Parsi, M., Agrawal, M., Srinivasan, V., Vieira, R., Torres, C., McLaury, B., Shirazi, S., Schleicher, E., Hampel, U., Assessment of a hybrid CFD model for simulation of complex vertical upward gas-liquid churn flow. *Chemical Engineering Research and Design*, 105, 71-84 (2016).
12. M. Abdulkadir, V. Hernandez-Perez, S. Lo, I. S. Lowndes, B. J. Azzopardi, Comparison of experimental and computational fluid dynamics (CFD) studies of slug flow in a vertical riser, *Experimental Thermal and Fluid Science* 68, 468483 (2015).
13. J. D. P. Araujo, J.M. Miranda, J. B. L. M. Campos, Flow of two consecutive Taylor bubbles through a vertical column of stagnant liquid: a CFD study about the influence of the leading bubble on the hydrodynamics of the trailing one, *Chemical Engineering Science*, 97 (2013) 1633.
14. E. Da Riva, D. Del Col, Numerical simulation of churn flow in a vertical pipe, *Chemical Engineering Science* 64 (17) (2009) 37533765.
15. N. Ratkovich, S. Majumder, T. R. Bentzen, Empirical correlations and CFD simulations of vertical two-phase gas liquid (Newtonian and non-Newtonian) slug flow compared against experimental data of void fraction, *Chemical Engineering Research and Design* 91 (6) (2013) 988998
16. Nakamura, T., Shiraishi, T., Ishitani, Y., Watakabe, H., Sago, H., Fujii, T., Yamaguchi, A., Konomura, M., Flow induced vibration of a large-diameter elbow piping based on random force measurement caused by conveying fluid (visualization test results). In: *Proceedings of PVP2005, 2005 ASME Pressure Vessels and Piping Division Conference*, Denver, Colorado USA, July 17-21 (2005)
17. Riverin, J. L., De Langre, E., Pettigrew, M. J. Fluctuating forces caused by internal two-phase flow on bends and tees, *Journal of Sound and Vibration*. 298, 1088-1098 (2006).
18. M. Ishii, T. Hibiki, *Thermo-fluid dynamics of two-phase flow*, Springer, New York, (2010).
19. D. L. Youngs, *Time-dependent multi-material flow with large fluid distortion*, Numerical Methods for Fluid Dynamics (1982).
20. H. K. Versteeg, W. Malalasekera, *An introduction to computational fluid dynamics, the finite volume method*, 2nd Edition, Pearson, England, (2007).
21. B. E. Launder, D. B. Spalding, The numerical computation of turbulent flows, *Computer methods in applied mechanics and engineering* 3 (1974) 269289.
22. Lowe, D. C. and Rezkallah, K. S., Flow regime identification in microgravity two-phase flows using void fraction signals, *Int. J. Multiphase Flow*, 25, 433-457 (1999).
23. Costigan G., Whalley P. B., Slug flow identification from dynamic void fraction measurements in vertical air-water flows, *Int. J. Multiphase Flow*, 23(2), 263-282 (1997).

24. Montoya, G., Lucas, D., Baglietto, E., Liao, Y., A review on mechanisms and models for the churn-turbulent flow regime, *Chemical Engineering Science*, 141, 86-103 (2016).
25. Abdulkadir, M., Hernandez-Perez, V., Lo, S., Lowndes, I. S., Azzopardi, B. J., Comparison of experimental and computational fluid dynamics (CFD) studies of slug flow in a vertical 90 bend. *The Journal of Computational Multiphase Flows*, 5(4), 265-281 (2013).